Korean J. Chem. Eng., 37(1), 37-45 (2020)
DOI: 10.1007/s11814-019-0416-6

pISSN: 0256-1115
eISSN: 1975-7220

The effects of radiation on heat and mass transfer of magnetohydrodynamic Marangoni flow in the boundary layer over a disk

Yanhai Lin† and Meng Yang

Fujian Province University Key Laboratory of Computation Science and School of Mathematical Sciences, Huaqiao University, Quanzhou 362021, P.R. China
(*Received 16 August 2019 • accepted 25 October 2019*)

Abstract−This study investigated the problem of radiation effects on the flow heat and mass transfer of magnetohydrodynamic steady laminar Marangoni convection in the boundary layer over a disk in the presence of a linear heat source and first-order chemical reactions. The governing partial differential equations of the disk model were established and transformed to a series of ordinary differential equations via suitable self-similar transformations, which were solved numerically by the shooting technique coupled with Runge-Kutta scheme and Newton's method. The Marangoni number related to temperature and concentration was derived, the effects of the magnetic Hartmann number, Marangoni number, radiation number, heat source number and chemical reaction number related to velocity, temperature, and concentration profiles were analyzed. The results demonstrate that the Hartmann number and Marangoni number have significant impacts on the heat and mass transfer of the Marangoni boundary layer flow. The temperature tends to increase with heat generation and decrease with heat absorption, and it exhibits a delay phenomenon for significant heat generation cases. Negative/positive chemical reactions tended to increase/decrease the concentration, similar to the effect of heat generation/absorption on the temperature.

Keywords: MHD, Marangoni Boundary Layer, Radiation Effect, Laminar Flow, Disk, Flow Heat Mass Transfer

INTRODUCTION

Marangoni convection appears owing to variations in surface tension on liquid-liquid or liquid-gas interfaces. The ubiquity of Marangoni convection is easily recognized in various fields of scientific research and engineering processes, such as growth and melting of semiconductor crystals, transmission of thin-liquid film, nucleation process of bubbles, liquid bridging, laser surface remelting, and material welding processing. For example, for liquid bridging, surface tension on the liquid-gas interface makes the liquid surface behave similarly to a thin elastic film, such that the surface morphology of the liquid bridge can be maintained without collapse. Arafune and Hirata [1] compared the interface velocities of thermal Marangoni boundary layer and solutal Marangoni boundary layer and concluded that the surface velocity of solutal Marangoni convection (50-200 mm/s) was about 3-5 times higher than that of thermal Marangoni convection (20-40 mm/s). Cazabat et al. [2] presented the fingering instability of spreading of thin-liquid films in the presence of Marangoni surface stress due to the temperature gradient. In addition, the Marangoni effect exists in both microgravity and earth gravity, which has been well reflected in space-based crystal growth experiments. Straub [3] also reported this finding through boiling tests under microgravity. During the nucleation process of bubbles, interface temperature and concentration along the bubble surface will change, thus causing Marangoni convection around bubbles [4,5]. Parra et al. [6] used bifurcation techniques to illustrate the effect of the Marangoni force on liquid bridging and determined an analytical relationship between parameters, through which variations of the maximum stable length could be predicted. Studies have demonstrated that Marangoni flow plays a very important role during laser surface remelting [7,8]. In general, the flow dynamics of a molten pool is driven by Marangoni force as well as buoyancy. The difference is that the former is caused by inhomogeneous heating along the interface, whereas the latter is caused by internal heat change [9]. Kim and Basu [10] investigated fluid flow and thermal behavior of a weld-pool under four driving forces. Their results revealed that electromagnetism and surface tension along with droplets had important effects on transfer behaviors of the weld-pool.

Liquid-gas or liquid-liquid interfaces can generate a dissipative layer, known as the Marangoni boundary layer. Recently, the fundamental mechanism of the Marangoni boundary layer has been broadly examined [11-13]. Christopher and Wang [4,5] first presented an estimated result of Marangoni convection around a vapor bubble. Similarity solutions of velocity field and the temperature field of Marangoni boundary layer flow caused by various imposed temperatures were given numerically. Pop and coworkers [14-19] investigated a series of characteristics of Marangoni boundary layers. Pop et al. [14] investigated the interaction between the thermal Marangoni convection and solute concentration Marangoni convection which can form along the surface. Chamkha et al. [15] explored coupled Marangoni mixed convection of two immiscible fluids in the presence of buoyancy effects as well as Marangoni effects. Saleem et al. [16] further investigated the Marangoni con-

†To whom correspondence should be addressed.
E-mail: linyanhai999@hqu.edu.cn

vection problem by extending it to an open-ended cavity when the energy of heated fluid was taken into account. Arifin et al. [17] considered thermal Marangoni convection of immiscible nanofluids with three different nanoparticles under the assumption of a strongly nonlinear power-law temperature gradient. Similarity transformation techniques and the shooting method were applied to get multiple (dual) solutions for the problem of Marangoni flow Navier-Stokes (N-S) equation, when the flow is induced due to a temperature gradient along the interface. They further investigated the problem considering radiation and suction/injection parameters [18]. Sheremet and Pop [19] numerically investigated the steady Marangoni natural convection process of a nanofluid within a heated cubical enclosure, considering that Brownian diffusion and thermophoresis were for the major slip mechanisms of nanoparticles. Mudhaf and Chamkha [20] reported on the numerical solution of thermosolutal Marangoni convection fluid flow. Based on the work of Christopher and Wang [4,5], both thermal and solutal Marangoni parameters were applied and uniform Loren magnetic force and linear chemical reaction process were considered. Later, they obtained exact parsing solutions for the Marangoni problem with Cardano's equations and Kummer's confluent hypergeometric function [21,22]. Zhang et al. [23,24] developed the double-parameter transformation perturbation expansion technique to scrutinize the approximate analytical expansions for the magnetohydrodynamic (MHD) thermosolutal Marangoni convection problem, in which the assumptions of the uniform Lorenz magnetic effect and linear chemical reaction process were held. Lin et al. [25-27] adopted the shooting method adopted for numerical solutions of the thermocapillary Marangoni convection fluid flow problem. The fluid flow of MHD non-Newtonian power law fluids driven by nonlinear temperature gradient was explored [25]. Later, pseudo-plastic non-Newtonian nanofluids with modified Fourier's heat transport process driven by radiation were examined [26]. The influence of copper water nanofluid particle shape on the Marangoni problem forced by a classical exponential decline temperature was explored [27]. Jiao et al. [28,29] applied the homotopy analysis method (HAM) to probe thermocapillary Marangoni flow and non-Fourier's heat transport of strongly non-Newtonian power law fluids. Using the same method, Sheikholeslami and Ganji [30,31] analytically presented the influence of the Lorentz force on Marangoni convection act of a copper-water nanofluid. Later, Sheikholeslami and Chamkha [32] examined the same problem in which the constitutive relationship of nanofluids was expressed by Buongiorno's model. Aly and Ebaid [33] obtained exact solutions for MHD Marangoni nanofluid flow driven by radiation effect using Laplace transformation. Hayat et al. [34] scrutinized the impact of SWCNT (single-wall-carbon-nano-tube) and MWCNT (multi-wall-carbon-nano-tube) on the Marangoni boundary layer problem of viscous non-Newtonian fluid considering the radiation effect in the energy expression. The mathematical model of fractional Maxwell fluid was established to study unsteady Marangoni convection fluid flow and non-Fourier heat transport by Zhao et al. [35] and a special fractional Marangoni boundary condition was adopted.

Recently, Lin and Zheng [36] showed the velocity distribution and temperature distribution for the Marangoni problem of copper-water (Cu) nanofluid at the interface of a porous medium infinite disk by using the cylindrical polar coordinate system and the generalized von Kármán transformation. They provided both analytical and numerical solutions. Later, Mahanthesh and coworkers [37-39] explored the thermal transport behaviors of Marangoni flow within nanofluids or Casson fluids. Mahanthesh and coworkers [37] showed the influence of solar radiation on the Marangoni problem across a flat interface utilizing a dusty nanoliquid driven by classical exponential space-dependent heat generation and absorption using a two-phase dusty fluid model. They also analyzed two-dimensional incompressible laminar Marangoni fluid flow of Cu/water nanoliquid over an infinite disk [38]. Thereafter, they presented exponential space dependent heat source (ESHS) and cross diffusion effects on MHD Marangoni boundary layer flow of a non-Newtonian Casson fluid on an infinite disk, considering Joule heating, viscous dissipation, and solar radiation.

Inspired by the aforementioned [36,38,39], we investigated the heat and mass transfer of MHD steady laminar Marangoni boundary layer fluid flow over a self-infinite disk. The thermal radiation term, a linear first-order chemical reaction process, and linear heat generation/absorption are considered. A series of suitable generalized Kármán transformations are applied to transform nonlinear governing partial differential equations (PDEs) to a series of ordinary differential equations (ODEs). Some important physical parameters, such as the radiation parameter and heat generation/absorption parameter, the two important Marangoni parameters, are given and discussed.

PHYSICAL MODELING AND SIMILARITY TRANSFORMATIONS

Consider the steady, laminar, two-dimensional, MHD Marangoni driven fluid flow transport process of an incompressible, electrically conducting fluid on a self-infinite disk. The fluid flow is motivated by surface tension due to the temperature gradient as well as concentration gradient. A linear heat source, a linear first-order chemical reaction and a uniform magnetic field normal to the interface disk are applied and the Hall effect is neglected [31,32]. Initially, the study fluid is stationary on the disk and the influence of the gravity also is neglected. A physical schematic with cylindrical polar coordinate system is established (Fig. 1). The Marangoni

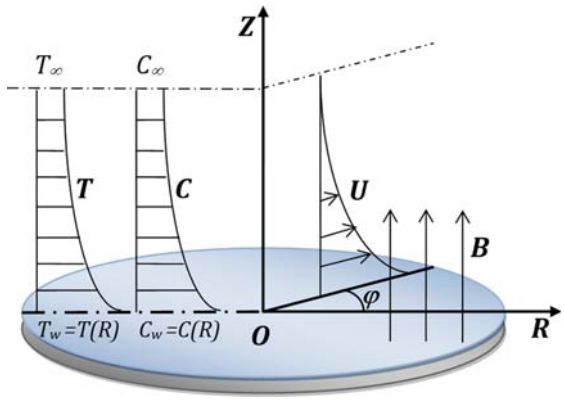

Fig. 1. Schematic of the physical system.

interface effect is considered as a boundary condition in the fluid flow modeling, which is different from the Boussinesq effect on the flow. According to the above hypotheses, the governing equations of the Marangoni boundary layer flow transport process can be given by [23,36,38,39]

$$\frac{\partial U}{\partial R}+\frac{U}{R}+\frac{\partial W}{\partial Z}=0, \tag{1}$$

$$U\frac{\partial U}{\partial R}+W\frac{\partial U}{\partial Z}=\frac{\mu\partial^2 U}{\rho\partial Z^2}-\frac{\delta B^2}{\rho}U, \tag{2}$$

$$U\frac{\partial T}{\partial R}+W\frac{\partial T}{\partial Z}=\alpha\frac{\partial^2 T}{\partial Z^2}+\frac{Q_0}{\rho c_p}(T-T_\infty)-\frac{1}{\rho c_p}\frac{\partial q_r}{\partial Z}, \tag{3}$$

$$U\frac{\partial C}{\partial R}+W\frac{\partial C}{\partial Z}=D\frac{\partial^2 C}{\partial Z^2}-G_0(C-C_\infty). \tag{4}$$

along with the following boundary conditions:

$$Z=0\text{: } W=0,\ \mu\frac{\partial U}{\partial Z}=\frac{\partial\sigma}{\partial R}, \tag{5}$$

$$T=T_w=T_\infty+AR^2,\ C=C_w=C_\infty+A^*R^2,$$

$$Z\to+\infty\text{: } U=U_\infty=0,\ T=T_\infty,\ C=C_\infty, \tag{6}$$

Here, U is the R-direction velocity and W is the Z-direction velocity. ρ and μ represent fluid density and kinematic viscosity, respectively. δ represents electrical conductivity and B represents magnetic induction. T is fluid temperature, C is concentration, α means the thermal diffusivity, Q_0 denotes the linear heating generation/absorption coefficient, T_∞ denotes temperature of fluid within potential flow area, which is a constant, and c_p is the specific heat. D denotes mass diffusivity, G_0 denotes chemical reaction process coefficient ($G_0>0$ is the positive chemical reaction, i.e., consumption of reactants, $G_0<0$ is the negative chemical reaction, i.e., generation of products) and C_∞ denotes the concentration of fluid within the potential flow area, which is also a constant. A and A^* are constants. q_r is radiative heat flux and it can be simplified as $q_r=-\frac{4\delta^*\partial T^4}{3k^*\partial Z}$ by applying the Rosseland approximation. Here, k^* and δ^* denote the mean absorption coefficient and the Stefan-Boltzmann constant. Under assumption of small temperature difference, the higher-order terms are neglected and T^4 can be approximated as $T^4\approx 4T_\infty^3T-3T_\infty^4$ [26,40]. We obtain the relationship between surface force and temperature/concentration by the following assumed expression [20-23]

$$\sigma=\sigma_0-\gamma_C(C-C_\infty)-\gamma_T(T-T_\infty),\ \frac{\partial\sigma}{\partial R}=\frac{\partial\sigma\partial C}{\partial C\partial R}+\frac{\partial\sigma\partial T}{\partial T\partial R}, \tag{7}$$

where, σ_0, γ_T and γ_C are positive constants.

Introducing dimensionless variables:

$$u=\frac{U}{U_\Delta},\ w=\frac{W}{U_\Delta}\sqrt{\frac{U_\Delta R_\Delta}{\gamma}}=\frac{W}{U_\Delta}\sqrt{Re}, \tag{8}$$

$$r=\frac{R}{R_\Delta},\ z=\frac{Z}{R_\Delta}\sqrt{\frac{U_\Delta R_\Delta}{\gamma}}=\frac{Z}{R_\Delta}\sqrt{Re}, \tag{9}$$

$$t=\frac{T-T_\infty}{T_\infty},\ c=\frac{C-C_\infty}{C_\infty}, \tag{10}$$

$$\gamma=\frac{\mu}{\rho},\ Re=\frac{U_\Delta R_\Delta}{\gamma},\ Pr=\frac{\gamma}{\alpha},\ Sc=\frac{\gamma}{D}, \tag{11}$$

where, U_Δ is unit velocity, R_Δ is unit length, Re denotes Reynolds number, γ is the kinematic viscosity, and Sc and Pr denote the Schmidt and Prandtl numbers. Substituting Eqs. (8)-(11) into governing Eqs. (1)-(4), the dimensionless equations are obtained.

$$\frac{\partial u}{\partial r}+\frac{u}{r}+\frac{\partial w}{\partial z}=0, \tag{12}$$

$$u\frac{\partial u}{\partial r}+w\frac{\partial u}{\partial z}=\frac{\partial^2 u}{\partial z^2}-\frac{\delta B^2R_\Delta}{\rho U_\Delta}u, \tag{13}$$

$$u\frac{\partial t}{\partial r}+w\frac{\partial t}{\partial z}=\frac{1}{Pr}\frac{\partial^2 t}{\partial z^2}+\frac{Q_0R_\Delta}{\rho C_pU_\Delta}t+\frac{1}{Pr}\frac{16\delta^*T_\infty^3}{3k^*\rho c_p\alpha}\frac{\partial^2 t}{\partial z^2}, \tag{14}$$

$$u\frac{\partial c}{\partial r}+w\frac{\partial c}{\partial z}=\frac{1}{Sc}\frac{\partial^2 c}{\partial z^2}-\frac{G_0R_\Delta}{U_\Delta}c. \tag{15}$$

The boundary conditions (5)-(6) are converted into Eqs. (16)-(17)

$$z=0\text{: }\left.\frac{\partial u}{\partial z}\right|_{z=0}=-\frac{1}{\mu U_\Delta}Re^{-\frac{1}{2}}\left(\gamma_TT_\infty\left.\frac{\partial t}{\partial r}\right|_{z=0}+\gamma_CC_\infty\left.\frac{\partial c}{\partial r}\right|_{z=0}\right),$$

$$w|_{z=0}=0,\ t|_{z=0}=\frac{AR_\Delta^2}{T_\infty}r^2,\ c|_{z=0}=\frac{A^*R_\Delta^2}{C_\infty}r^2, \tag{16}$$

$$z\to+\infty\text{: }u|_{z\to+\infty}=0,\ t|_{z\to+\infty}=0,\ c|_{z\to+\infty}=0. \tag{17}$$

Introducing the dimensionless generalized Kármán similarity variable and dimensionless number as

$$\xi=Ez,\ u=E^2rF(\xi),\ w=EH(\xi),\ E=\sqrt{\frac{\gamma}{U_\Delta R_\Delta}}=Re^{-\frac{1}{2}}, \tag{18}$$

$$t=\frac{AR_\Delta^2}{T_\infty}r^2\theta(\xi),\ c=\frac{A^*R_\Delta^2}{C_\infty}r^2\phi(\xi), \tag{19}$$

$$Ha=\frac{\delta R_\Delta^2B^2}{\mu},\ Nr=\frac{16\delta^*T_\infty^3}{3k^*\rho c_p\alpha},\ Q=\frac{Q_0R_\Delta^2}{\rho c_p\gamma},\ G=\frac{G_0R_\Delta^2}{\gamma}, \tag{20}$$

$$Ma_T=\frac{2\gamma_TAR_\Delta^3}{\mu\alpha}\propto\frac{\gamma_T\Delta TL}{\mu\alpha},\ Ma_C=\frac{2\gamma_CA^*R_\Delta^3}{\mu D}\propto\frac{\gamma_C\Delta CL}{\mu D}, \tag{21}$$

where, Ha is Hartmann number, Nr is the radiation parameter, G denotes the chemical reaction parameter, and Q denotes the heat generation/absorption parameter. Ma_T and Ma_C represent the thermal Marangoni number and solutal Marangoni number, respectively. Ma denotes the Marangoni number. Then, Eqs. (12)-(15) are converted into Eqs. (22)-(25):

$$2F(\xi)+H'(\xi)=0, \tag{22}$$

$$F''(\xi)=F^2(\xi)+H(\xi)F'(\xi)+HaF(\xi), \tag{23}$$

$$\theta''(\xi)=\frac{Pr}{1+Nr}[2F(\xi)\theta(\xi)+H(\xi)\theta'(\xi)-Q\theta(\xi)], \tag{24}$$

$$\phi''(\xi)=Sc[2F(\xi)\phi(\xi)+H(\xi)\phi'(\xi)+G\phi(\xi)]. \tag{25}$$

The boundary conditions (16)-(17) are reduced as:

$$F'(0)=-\left(\frac{Ma_T}{Pr}+\frac{Ma_C}{Sc}\right)=-Ma,\ H(0)=0,\ F(+\infty)=0, \tag{26}$$

$$\theta(0)=1,\ \theta(+\infty)=0, \tag{27}$$

$$\phi(0)=1,\ \phi(+\infty)=0. \tag{28}$$

Using the above dimensionless variables and generalized dimensionless Kármán similarity variable, the velocity, shear stress, temperature, and concentration can be given as (assuming that (R_{real}, Z_{real}) is any point in the flow field over the disk)

$$\xi_{real}=\frac{Z_{real}}{R_\Delta}\sqrt{\frac{U_\Delta R_\Delta}{\gamma}}E=\frac{Z_{real}}{R_\Delta}, \tag{29}$$

$$U=\frac{\gamma}{R_\Delta^2}R_{real}F(\xi_{real}),\ W=\frac{\gamma}{R_\Delta}H(\xi_{real}),\ \tau=\frac{\rho\gamma^2}{U_\Delta R_\Delta}R_{real}F'(\xi_{real}), \tag{30}$$

$$T=T_\infty+AR_{real}^2\theta(\xi_{real}),\ C=C_\infty+A^*R_{real}^2\phi(\xi_{real}), \tag{31}$$

Here, the dimensionless radial velocity and the dimensionless vertical velocity are expressed by $F(\xi)$ and $H(\xi)$, respectively. $F'(\xi)$ denotes the dimensionless shear force. The dimensionless fluid temperature and dimensionless concentration are defined by $\phi(\xi)$ and $\theta(\xi)$, respectively.

NUMERICAL CALCULATION PROCESS

1. Simplification of Equations

The shooting technique combined with the Runge-Kutta method and Newton's iteration scheme is used to achieve the goal of obtaining solutions of the simplified Eqs. (22)-(25) together with the corresponding boundary conditions (26)-(27). Therefore, the dimensionless simplified ODEs are first transformed into a one-order ODE boundary-value problem. Redefine F′, θ', and ϕ' as I, J, and L as follows:

$$H'(\xi)=-2F(\xi),\ F'(\xi)=I(\xi),\ I'(\xi)=F^2(\xi)+H(\xi)I(\xi)+HaF(\xi), \tag{32}$$

$$\theta'(\xi)=J(\xi),\ J'(\xi)=\frac{Pr}{1+Nr}[2F(\xi)\theta(\xi)+H(\xi)J(\xi)-Q\theta(\xi)], \tag{33}$$

$$\phi'(\xi)=L(\xi),\ L'(\xi)=Sc[2F(\xi)\phi(\xi)+H(\xi)L(\xi)+G\theta(\xi)]. \tag{34}$$

which satisfy the following new boundary conditions:

$$F(0)=-Ma,\ H(0)=0,\ F(\infty)=0, \tag{35}$$

$$\theta(0)=1,\ \theta(\infty)=0, \tag{36}$$

$$\phi(0)=1,\ \phi(\infty)=0. \tag{37}$$

Introducing the shooting parameters i, j, and l as

$$I(0)=i,\ J(0)=j,\ L(0)=l. \tag{38}$$

Eqs. (32)-(36) are converted into Eqs. (39)-(44)

$$\left(\frac{\partial H}{\partial i}\right)'=\frac{\partial H'}{\partial i}=-2\frac{\partial F}{\partial i},\ \left(\frac{\partial F}{\partial i}\right)'=\frac{\partial(F')}{\partial i}=\frac{\partial I}{\partial i},$$
$$\left(\frac{\partial I}{\partial i}\right)'=\frac{\partial(I')}{\partial i}=2F\frac{\partial F}{\partial i}+H\frac{\partial I}{\partial i}+I\frac{\partial H}{\partial i}+Ha\frac{\partial F}{\partial i}, \tag{39}$$

$$\left(\frac{\partial\theta}{\partial j}\right)'=\frac{\partial(\theta')}{\partial j}=\frac{\partial J}{\partial j},$$
$$\left(\frac{\partial J}{\partial j}\right)'=\frac{\partial(J')}{\partial j}=\frac{Pr}{1+Nr}\left(2F\frac{\partial\theta}{\partial j}+2\theta\frac{\partial F}{\partial j}+H\frac{\partial J}{\partial j}+J\frac{\partial H}{\partial j}-Q\frac{\partial\theta}{\partial j}\right) \tag{40}$$

$$\left(\frac{\partial\phi}{\partial l}\right)'=\frac{\partial(\phi')}{\partial l}=\frac{\partial L}{\partial l},$$
$$\left(\frac{\partial L}{\partial l}\right)'=\frac{\partial(L')}{\partial l}=Sc\left(2F\frac{\partial\phi}{\partial l}+2\phi\frac{\partial F}{\partial l}+H\frac{\partial L}{\partial l}+L\frac{\partial H}{\partial l}+G\frac{\partial\phi}{\partial l}\right) \tag{41}$$

$$\left.\frac{\partial H}{\partial i}\right|_{\eta=0}=0,\ \left.\frac{\partial F}{\partial i}\right|_{\eta=0}=1,\ \left.\frac{\partial I}{\partial i}\right|_{\eta=0}=0, \tag{42}$$

$$\left.\frac{\partial\theta}{\partial j}\right|_{\eta=0}=0,\ \left.\frac{\partial J}{\partial j}\right|_{\eta=0}=1, \tag{43}$$

$$\left.\frac{\partial\phi}{\partial l}\right|_{\eta=0}=0,\ \left.\frac{\partial L}{\partial l}\right|_{\eta=0}=1. \tag{44}$$

2. Programming Approach

The boundary-value problem (25)-(28) can be solved numerically by the shooting technique combined with the Runge-Kutta method and Newton's iteration scheme. The detailed process is as follows:

(1) Provide initial values for the shooting parameters $I(0)=i_0$, $J(0)=j_0$ and $L(0)=l_0$.

(2) Utilize the classical 4th-order Runge-Kutta technique to solve problems (32)-(37) and denote the results as $\{H^1, F^1, I^1, \theta^1, J^1, \phi^1, L^1\}$.

(3) Present the test results as $|F(\infty)|<\varepsilon$, $|\theta(\infty)|<\varepsilon$ and $|\phi(\infty)|<\varepsilon$, where ε represents the iteration accuracy. The iteration loop is over as long as the calculated solutions of the step two satisfy the test results, and $\{H^1, F^1, I^1, \theta^1, J^1, \phi^1, L^1\}$ is the solution of the equations. If not, step three will be executed.

(4) Apply Newton's iteration scheme to modify the initial values:

$$i_{k+1}=i_k-\frac{I(i_k)}{\partial I(i_k)/\partial i_k},\ j_{k+1}=j_k-\frac{J(j_k)}{\partial J(j_k)/\partial j_k},\ l_{k+1}=l_k-\frac{L(l_k)}{\partial L(l_k)/\partial l_k}. \tag{45}$$

Eqs. (39)-(44) are used to obtain the items $\partial I(i_k)/\partial i_k$, $\partial J(J_k)/\partial j_k$, and $\partial L(l_k)/\partial l_k$ in fixed Eq. (45). Until the modified solutions of the step two satisfy the test results, the steps one to three will be repeated.

Table 1. Comparison of values of F(0), H(∞), $-\theta'(0)$ and $-\phi'(0)$ for Ma=0.2, Pr=7.0, Sc=0.6, and Ha=Nr=Q=G=0

	Ref. [36] (HAM)	Ref. [36] (Numerical)	RKF-45 [39]	Present results
F(0)	0.307593	0.3073370	0.3074672	0.3073401
$-H(\infty)$	0.835982	0.8316574	0.8335362	0.8318683
$-\theta'(0)$	2.42527	2.428746	2.427856	2.428761
$-\phi'(0)$	\	\	0.5812643	0.5816996

Table 2. Values of F(0), $-\theta'(0)$ and $-\phi'(0)$ for different values of Ha when Ma=5, Pr=0.78, Sc=0.6, and Nr=Q=G=0

	Ha=0	Ha=1	Ha=2	Ha=3	Ha=4
F(0)	2.627829	2.411974	2.229207	2.074461	1.942790
$-\theta'(0)$	2.015047	1.868791	1.734875	1.613323	1.503524
$-\phi'(0)$	1.697931	1.566191	1.445839	1.337058	1.239492

Table 3. Values of F(0), $-\theta'(0)$ and $-\phi'(0)$ for different values of Ma when Ha=0, Pr=0.78, Sc=0.6, and Nr=Q=G=0

	Ma=2	Ma=4	Ma=6	Ma=8
F(0)	1.426633	2. 264629	2.967505	3.594877
$-\theta'(0)$	1.485052	1.871173	2.142064	2.357737
$-\phi'(0)$	1.253701	1.580705	1.810382	1.993387

RESULTS AND DISCUSSION

This work presents an MHD Marangoni driven fluid flow transport problem over a disk with radiation effects, linear heat generation/absorption, and linear first-order chemical reaction. To verify the accuracy and effectiveness of the present method, the results for degradation (Ma=0.2, Ha=0, Nr=0, Pr=7.0, Q=0, Sc=0.6, G=0) are presented with those in Refs. [36,39] in Table 1. A series of tables and graphs were generated to illustrate the impacts of various parameters on the Marangoni fluid flow problem.

Influences of Hartmann number and Marangoni number on F(0), $-\theta'(0)$, and $-\phi(0)$ are shown in Tables 2 and 3, respectively, when other physical parameters are fixed. Using the similarity transformations and Eqs. (29)-(31), we can get

$$\begin{cases} U(0)=\dfrac{\gamma}{R_{\Delta}^{2}}R_{real}F(0), \\ Nu_{X}=-\dfrac{R_{\Delta}}{T_{w}-T_{\infty}}\left(\dfrac{\partial T}{\partial Z}\right)_{Z=0}=-\theta'(0), \\ Sh_{X}=-\dfrac{R_{\Delta}}{C_{w}-C_{\infty}}\left(\dfrac{\partial C}{\partial Z}\right)_{Z=0}=-\phi'(0), \end{cases}$$

where, F(0) is the dimensionless interface radial velocity, $-\theta(0)$ is the local Nusselt number, and $-\phi'(0)$ is the local Sherwood number. From these tables, we can observe that F(0) decreases, while $-\theta(0)$ and $-\phi'(0)$ increase with increasing Hartmann number. However, F(0) increases, while $-\theta(0)$ and $-\phi'(0)$ decrease with increasing Marangoni number.

Figs. 2-6 show impacts of the Hartmann number Ha on various dimensionless functions, such as radial velocity $F(\xi)$, vertical velocity $H(\xi)$, shear stress $F'(\xi)$, temperature $\theta(\xi)$, and concentration $\phi(\xi)$ for Ma=5, Pr=0.78, Sc=0.6, and Nr=Q=G=0. In the physical model, the existence of a magnetic field vertical to the disk interface caused a drag-like force, which we call the Lorentz force. The results indicate that the force typically slows down fluid flow along the interface and increases fluid temperature and concentration simultaneously [20-22]. These figures show that as the Hartmann number increases, the radial velocity, vertical velocity, and shear stress decrease with increasing temperature and concentration. These tendencies are in agreement with the role of the magnetic field. Furthermore, the increase of the magnetic field intensity leads to increases in temperature and concentration boundary layers but a decrease in hydrodynamic velocity boundary layer. These trends of the disk and previous conclusions for a flat surface are similar (Mudhaf and Chamkha [20]).

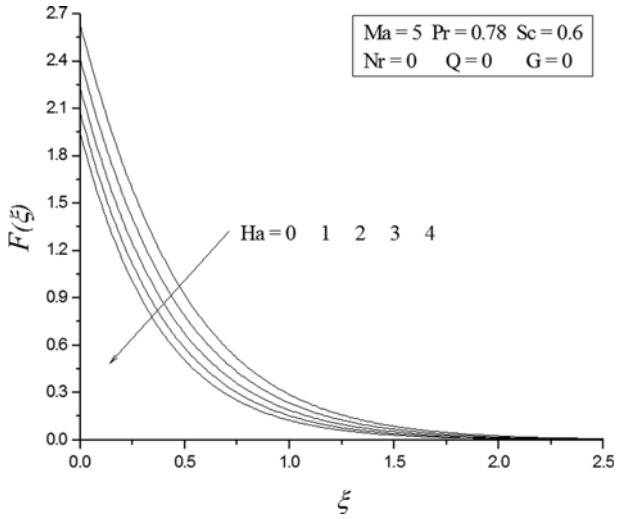

Fig. 2. Effects of the Hartmann number on F(ξ).

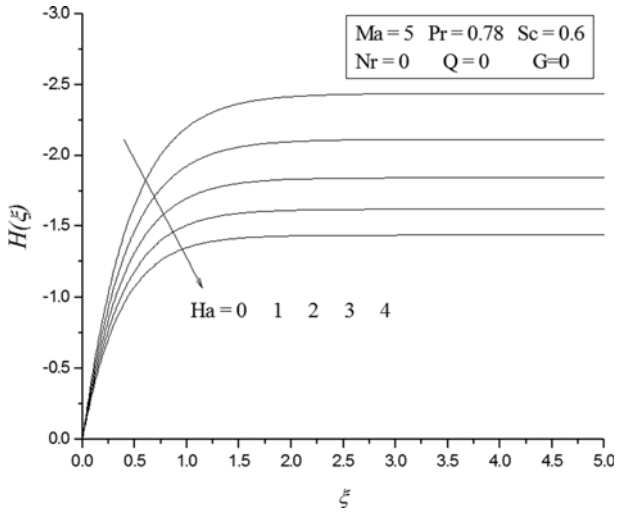

Fig. 3. Effects of the Hartmann number on H(ξ).

Figs. 7-11 present influences of the Marangoni number Ma on the above dimensionless function for Ha=0, Pr=0.78, Sc=0.6 and Nr=Q=G=0. In the Marangoni driven boundary layer problem, the Marangoni interface effect serves as a boundary-condition in fluid

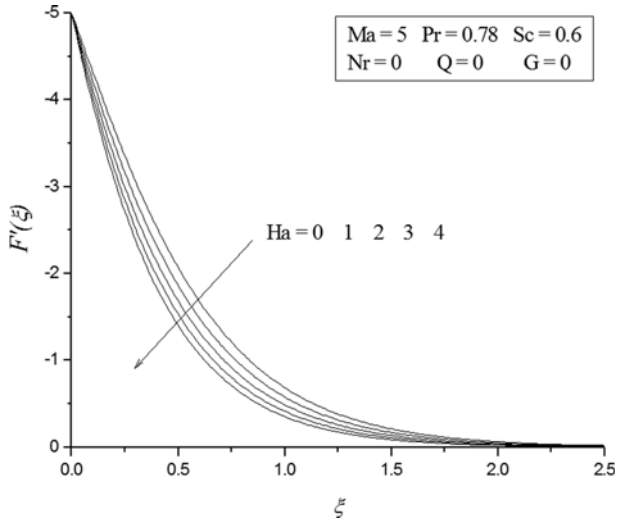

Fig. 4. Effects of the Hartmann number on F′(ξ).

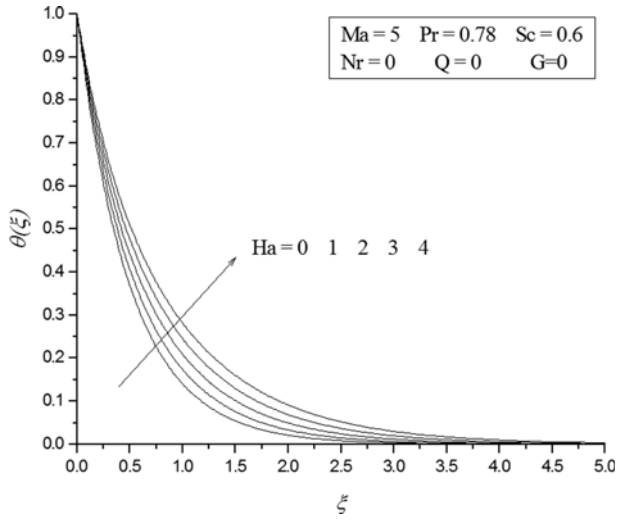

Fig. 5. Effects of the Hartmann number on θ(ξ).

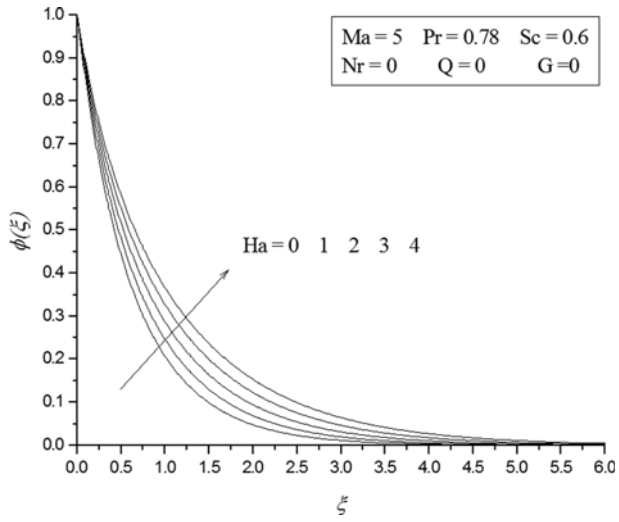

Fig. 6. Effects of the Hartmann number on ϕ(ξ).

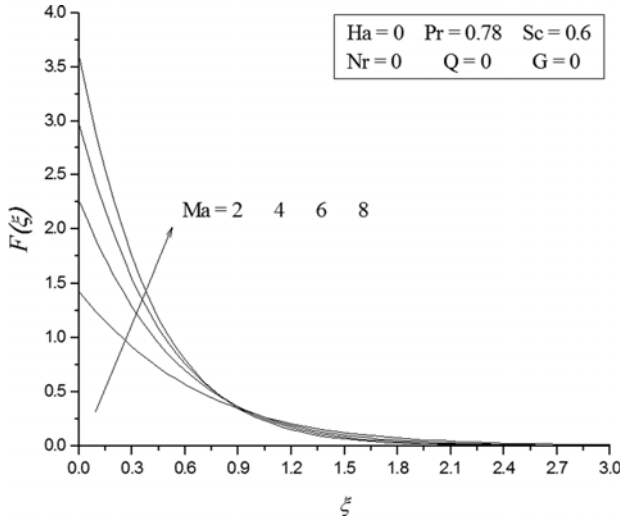

Fig. 7. Effects of the Marangoni number on F(ξ).

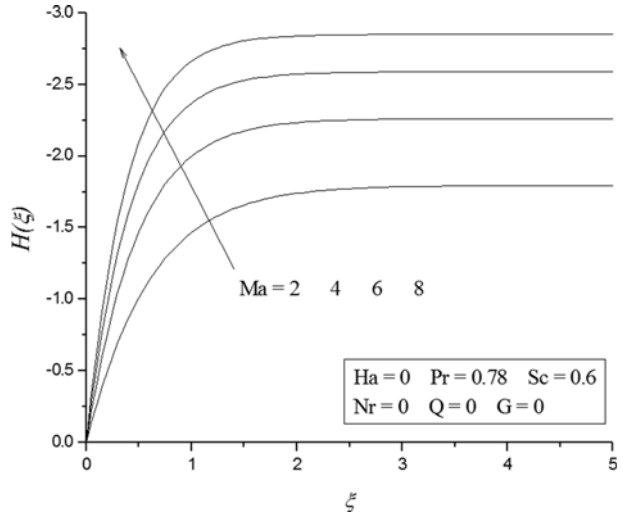

Fig. 8. Effects of the Marangoni number on H(ξ).

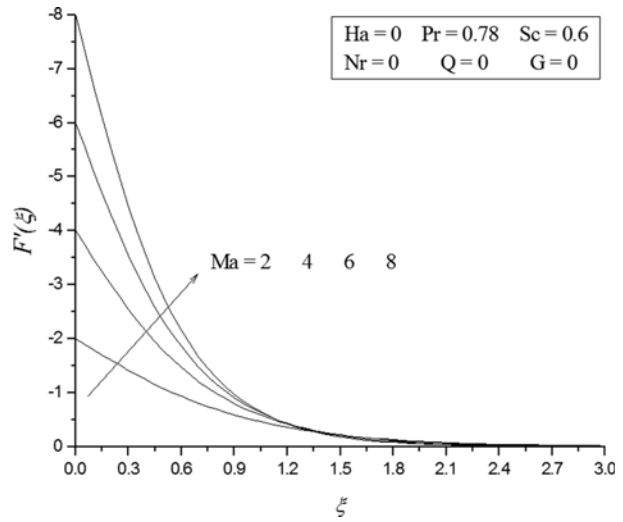

Fig. 9. Effects of the Marangoni number on F′(ξ).

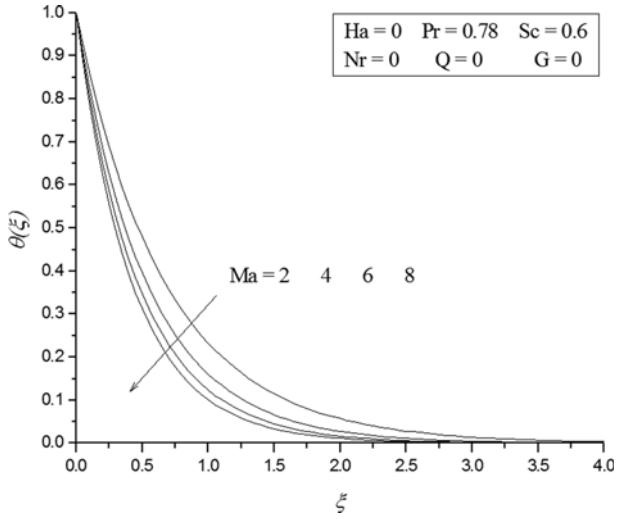

Fig. 10. Effects of the Marangoni number on $\theta(\xi)$.

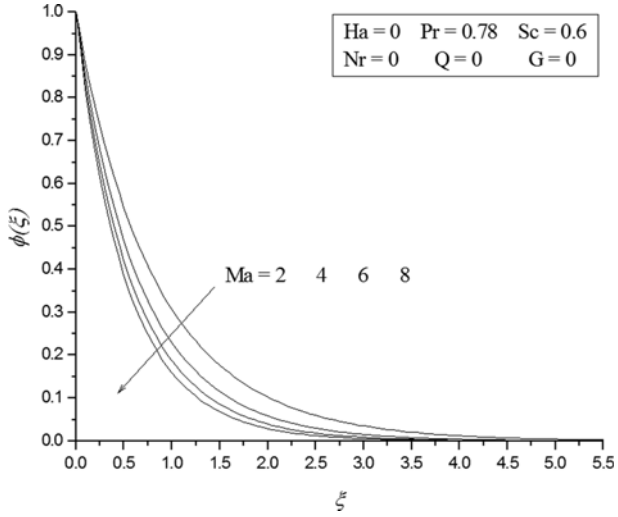

Fig. 11. Effects of the Marangoni number on $\phi(\xi)$.

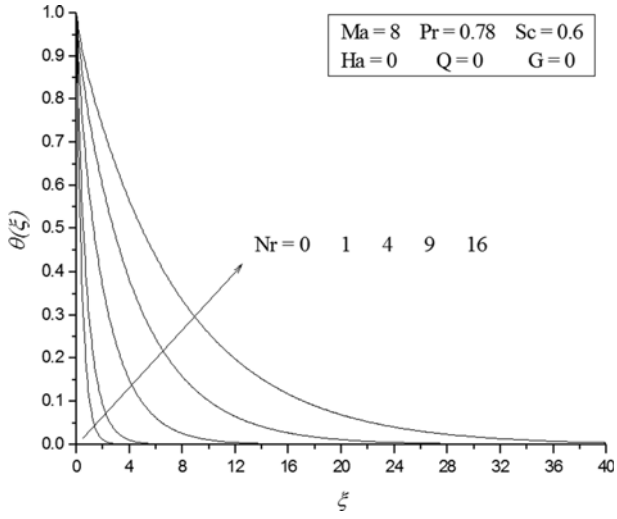

Fig. 12. Effects of the radiation parameter on $\theta(\xi)$.

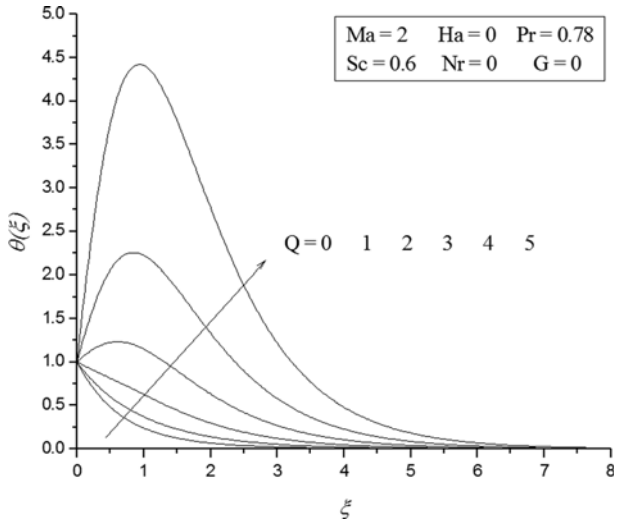

Fig. 13. Effects of the heat source parameter (heat generation) on $\theta(\xi)$.

flow model PDEs. Marangoni flow over the disk is driven by a combination of the interface temperature and concentration gradients. Thus, the Marangoni number was derived as $\mathrm{Ma}=\frac{\mathrm{Ma}_T}{\mathrm{Pr}}+\frac{\mathrm{Ma}_C}{\mathrm{Sc}}$ (Section 2). Thus, the Marangoni number represents the interface Marangoni driving force. Figs. 7-9 show that the location similarity variable ξ increases when the radial velocity as well as the shear stress decrease. Furthermore, the values of the vertical velocity $H(\xi)$ and shear stress $F'(\xi)$ are non-positive. The characteristics of the Marangoni boundary layer problem are in good agreement with these trends. In addition, it is significant that the vertical velocity increases as the Marangoni number increases, which is contrary to the trend of temperature and concentration. Furthermore, shear stress and radial velocity in the outer part of the boundary layer appear to decrease, whereas interface velocity and interface shear stress increase as the Marangoni number increases. Accordingly, the hydrodynamics, temperature, and concentration boundary layer decrease with increasing Marangoni number. Furthermore, Fig. 7 shows that the range around $\xi\approx$0.7-1.1 can lead to intersections of $F(\xi)$ in the near-surface region for the specified parameters. Fig. 9 also shows that these intersections of $F'(\xi)$ can still occur within the range around $\xi\approx$1.0-1.8 for the specified parameters.

Figs. 12-14 present influences of the radiation parameter Nr and heat generation/absorption parameter Q on $\theta(\xi)$ for Ma=8, Pr=0.78, Sc=0.6, Ha=Q=G=0, and Ha=Nr=G=0, respectively. As the radiation parameter increases, the dimensionless fluid temperature increases. In addition, the fluid temperature and temperature boundary-layer increase as heat generation/absorption increases. In the case of heat absorption (Q<0), the fluid temperature quickly decreases from 1 to 0 and the rate of decline increases with enhanced heat absorption. So, the decrease in fluid temperature is affected by heat absorption. For heat generation (Q>0), the temperature also generally decreases from 1 to 0 and the rate of decline decreases with enhanced heat generation, so the heat generation case has an impulse to raise temperature. Furthermore, the temperature

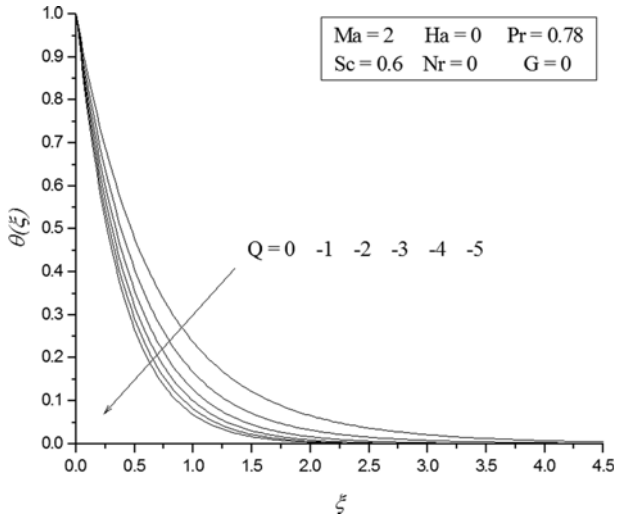

Fig. 14. Effects of the heat source parameter (heat absorption) on $\theta(\xi)$.

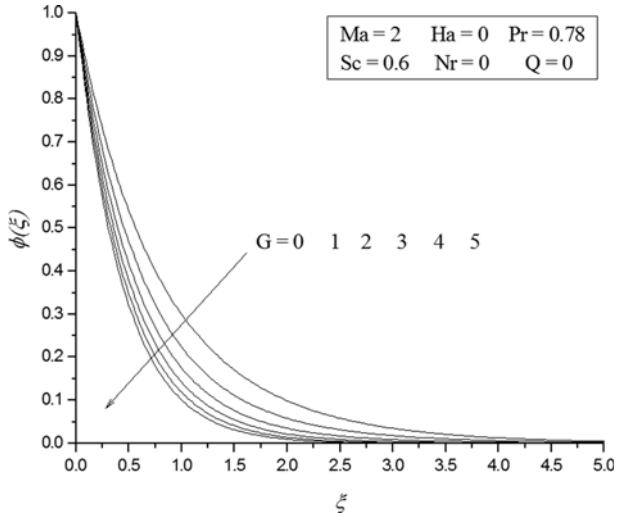

Fig. 15. Effects of the chemical reaction parameter (positive chemical reaction) on $\phi(\xi)$.

distribution shows a delay phenomenon for cases of significant heat generation. The temperature of the fluid initially increases with ξ, and then gradually decreases to zero after reaching a maximum. The higher the value of heat generation/absorption, the higher the maximum temperature.

Figs. 15-16 present the influence of the chemical reaction parameter G on the dimensionless concentration $\phi(\xi)$ for Ma=2, Pr=0.78, Sc=0.6, and Ha=Nr=Q=0. Both concentration and thickness of the concentration boundary-layer appear to increase with decreasing chemical reaction. For the positive chemical reaction (G>0), the concentration rapidly declines from 1 to 0 and the rate of decline increases with enhanced positive chemical reaction. The positive chemical reaction thus tends to reduce the fluid concentration. For the negative chemical reaction (G<0), the concentration also generally declines from 1 to 0 and the rate of decline decreases with enhanced negative chemical reaction: The negative chemical reaction thus tends to increase the fluid concentration. Furthermore, the concentration shows a delay phenomenon for cases of significant negative chemical reaction. As ξ increases, the concentration of the fluid initially increases to its maximum value and then slowly decreases to zero. The higher the value of chemical reaction, the higher the maximum concentration.

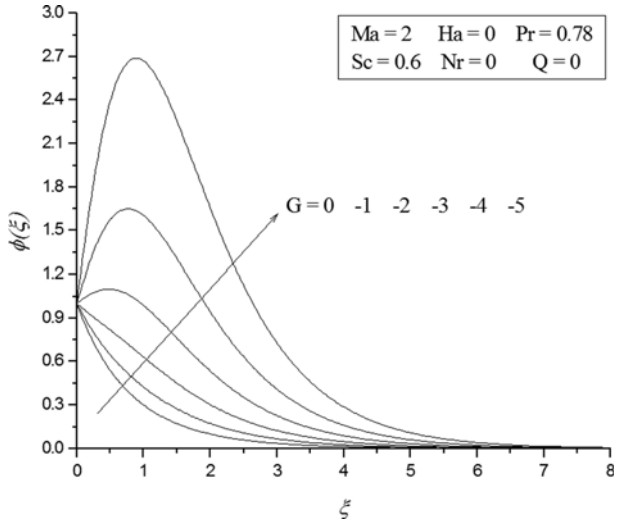

Fig. 16. Effects of the chemical reaction parameter (negative chemical reaction) on $\phi(\xi)$.

CONCLUSIONS

This research presents radiation effects on the heat and mass transfer of MHD Marangoni boundary layer flow over a disk. To this end, thermal radiation effects, a linear heat source and a linear first-order chemical reaction process were considered. A complex problem was created and the N-S and thermal/solutal equations were converted into an ordinary differential equations boundary-value problem using suitable self-similar transformations. Furthermore, the Marangoni number related to temperature and concentration was derived. The following conclusions can be drawn:

(a) As the Hartmann number increases, the velocity and shear stress decrease, while temperature and concentration increase.

(b) As the Marangoni number increases, the interface radial velocity and interface shear driven force increase, while temperature and concentration decrease.

(c) As the radiation effect increases, the temperature of the fluid increases.

(d) Heat generation has a tendency to increase fluid temperature, whereas heat absorption has the opposite tendency. Temperature shows a delay phenomenon for cases of significant heat generation.

(e) Negative chemical reaction has a tendency to increase fluid concentration, whereas positive chemical reaction reduces it. Concentration shows a delay phenomenon for cases with significant negative chemical reaction.

ACKNOWLEDGEMENTS

Yanhai Lin was supported by the National Natural Science Foun-

dations of China (Nos. 11702101 and 11626106), the Fundamental Research Funds for the Central Universities and the Promotion Program for Young and Middle-aged Teacher in Science and Technology Research of Huaqiao University (No. ZQN-PY502), the Natural Science Foundation of Fujian Province (No. 2019J05093) and Quanzhou High-Level Talents Support Plan. Meng Yang was supported by the Subsidized Project for Postgraduates' Innovative Fund in Scientific Research of Huaqiao University.

REFERENCES

1. K. Arafune and A. Hirata, *J. Cryst. Growth*, **197**, 811 (1999).
2. A. M. Cazabat, F. Heslot, S. M. Troian and P. Carles, *Nature*, **346**, 824 (1990).
3. J. Straub, *Exp. Therm. Fluid Sci.*, **9**(3), 253 (1994).
4. D. M. Christopher and B. X. Wang, *Int. J. Heat Mass Trans.*, **44**, 799 (2001).
5. D. M. Christopher and B. X. Wang, *Int. J. Therm. Sci.*, **40**, 564 (2001).
6. I. E. Parra, J. M. Perales and J. Meseguer, *Adv. Space Res.*, **29**(4), 625 (2002).
7. Y. P. Lei, H. Murakawa, Y. W. Shi and X. Y. Li, *Comput. Mater. Sci.*, **21**, 276 (2001).
8. L. X. Yang, X. F. Peng and B. X. Wang, *Int. J. Heat Mass Trans.*, **44**, 4465 (2001).
9. P. J. Modenesi, E. R. Apolinário and I. M. Pereira, *J. Mater. Process. Technol.*, **99**, 260 (2000).
10. I. S. Kim and A. Basu, *J. Mater. Process. Technol.*, **77**, 17 (1998).
11. J. R. A. Pearson, *J. Fluid Mech.*, **4**(5), 489 (1958).
12. L. E. Scriven and C. V. Strenling, *Nature*, **187**, 186 (1960).
13. L. G. Napolitano, Marangoni boundary layers. In: Proceedings of the 3rd European Symposium on Material Science in Space, Grenoble, ESA SP-142, JUNE 1979.
14. I. Pop, A. Postelnicu and T. Grosan, *Meccanica*, **36**, 555 (2001).
15. A. J. Chamkha, I. Pop and H. S. Takhar, *Meccanica*, **41**, 219 (2006).
16. M. Saleem, M. A. Hossain, S. Mahmud and I. Pop, *Int. J. Heat Mass Trans.*, **54**, 4473 (2011).
17. N. M. Arifin, R. Nazar and I. Pop, *Meccanica*, **46**, 833 (2011).
18. N. A. Mat, N. M. Arifin, R. Nazar, F. Ismail and I. Pop, *Meccanica*, **48**, 83 (2013).
19. M. A. Sheremet and I. Pop, *J. Therm. Anal. Calorim.*, **135**(1), 357 (2019).
20. A. A. Mudhaf and A. J. Chamkha, *Heat Mass Transfer*, **42**, 112 (2005).
21. E. Magyari and A. J. Chamkha, *Heat Mass Transfer*, **43**, 965 (2007).
22. E. Magyari and A. J. Chamkha, *Int. J. Therm. Sci.*, **47**, 848 (2008).
23. Y. Zhang and L. C. Zheng, *Chem. Eng. Sci.*, **69**, 449 (2012).
24. Y. Zhang and L. C. Zheng, *Chinese J. Chem. Eng.*, **22**(4), 365 (2014).
25. Y. H. Lin, L. C. Zheng and X. X. Zhang, *J. Heat Transfer*, **135**, 051702 (2013).
26. Y. H. Lin, L. C. Zheng and X. X. Zhang, *Int. J. Heat Mass Trans.*, **77**, 708 (2014).
27. Y. H. Lin, B. T. Li, L. C. Zheng and G. Chen, *Powder Technol.*, **301**, 379 (2016).
28. C. R. Jiao, L. C. Zheng, Y. H. Lin, L. X. Ma and G. Chen, *Int. J. Heat Mass Trans.*, **92**, 700 (2016).
29. L. C. Zheng, C. R. Jiao, Y. H. Lin and L. X. Ma, *Heat Transfer Eng.*, **38**(6), 641 (2017).
30. M. Sheikholeslami and D. D. Ganji, *Indian J. Phys.*, **91**(12), 1581 (2017).
31. M. Sheikholeslami and D. D. Ganji, *Int. J. Hydrog. Energy*, **42**, 2748 (2017).
32. M. Sheikholeslami and A. J. Chamkha, *J. Mol. Liq.*, **225**, 750 (2017).
33. E. H. Aly and A. Ebaid, *J. Mol. Liq.*, **215**, 625 (2016).
34. T. Hayat, M. I. Khan, M. Farooq, A. Alsaedi and T. Yasmeen, *Int. J. Heat Mass Trans.*, **106**, 810 (2017).
35. J. H. Zhao, L. C. Zheng, X. H. Chen, X. X. Zhang and F. W. Liu, *Appl. Math. Model.*, **44**, 497 (2017).
36. Y. H. Lin and L. C. Zheng, *AIP Advances*, **5**, 107225 (2015).
37. B. Mahanthesh, B. J. Gireesha, B. C. Prasannakumara and N. S. Shashikumar, *Nucl. Eng. Technol.*, **49**, 1660 (2017).
38. B. Mahanthesh, B. J. Gireesha, B. C. Prasannakumara and P. B. Sampathkumar, *Results Phys.*, **7**, 2990 (2017).
39. B. Mahanthesh, B. J. Gireesha, N. S. Shashikumar, T. Hayat and A. Alsaedi, *Results Phys.*, **9**, 78 (2018).
40. B. Mahanthesh and B. J. Gireesha, *Results Phys.*, **8**, 869 (2018).